

Elastic Properties of GaN Nanowires: Revealing the Influence of Planar Defects on Young's Modulus at Nanoscale

Sheng Dai,[†] Jiong Zhao,[†] Mo-rigen He,[†] Xiaoguang Wang,[‡] Jingchun Wan,[‡] Zhiwei Shan,[‡] and Jing Zhu^{*†}

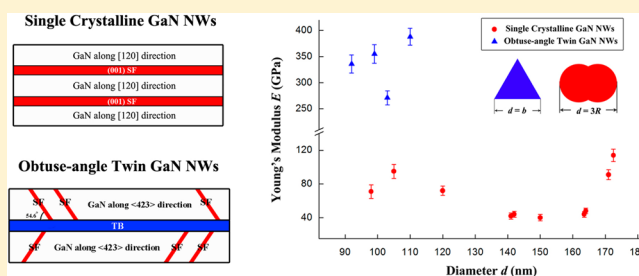
[†]Beijing National Center for Electron Microscopy, The State Key Laboratory of New Ceramics and Fine Processing, Laboratory of Advanced Materials, School of Materials Science and Engineering, Tsinghua University, Beijing 100084, China

[‡]Center for Advancing Materials Performance from the Nanoscale (CAMP-Nano) and Hysitron Applied Research Center in China (HARCC), State Key Laboratory for Mechanical Behavior of Materials, Xi'an Jiaotong University, Xi'an 710049, China

S Supporting Information

ABSTRACT: The elastic properties of gallium nitride (GaN) nanowires with different structures were investigated by in situ electron microscopy in this work. The electric-field-induced resonance method was utilized to reveal that the single crystalline GaN nanowires, along [120] direction, had the similar Young's modulus as the bulk value at the diameter ranging 92–110 nm. Meanwhile, the elastic behavior of the obtuse-angle twin (OT) GaN nanowires was disclosed both by the in situ SEM resonance technique and in situ transmission electron microscopy tensile test for the first time. Our results showed that the average Young's modulus of these OT nanowires was greatly decreased to about 66 GPa and indicated no size dependence at the diameter ranging 98–171 nm. A quantitative explanation for this phenomenon is proposed based on the rules of mixtures in classical mechanics. It is revealed that the elastic modulus of one-dimensional nanomaterials is dependent on the relative orientations and the volume fractions of the planar defects.

KEYWORDS: GaN nanowires, in situ electron microscopy, elastic behavior, Young's modulus, planar defects



Because of the various remarkable properties, gallium nitride (GaN), a technologically important semiconductor has ignited the research attention in recent years.¹ Bulk GaN exhibits excellent chemical inertness,² thermal stability,³ and a high piezoelectric constant⁴ so that it is used in high-temperature and high-power electronics.^{5,6} GaN nanowires (NWs) have also been investigated extensively and proved to process enhanced physical properties and nanodevice applications.^{7–13} However, compared to the well-known optoelectronic and photonic properties, relatively little has been understood about the mechanical properties of GaN NWs.

The study on the mechanical properties of GaN NWs is essential and imperative for the applications in GaN-NW-based devices. For example, it is necessary to know the accurate mechanical response of an individual GaN NW for its piezoelectric applications.^{14,15} For the optoelectronic and electric applications,^{9,10} GaN NWs may be subjected to their mechanical properties during the processing and working. For these reasons, several in situ techniques have been developed to investigate both elastic and plastic behaviors of GaN NWs. For instance, the in situ electric-field-induced resonance method has been utilized to explore the size dependence of Young's modulus in *m*-axis (the <120> direction) GaN NWs.^{16,17} Three-point bending tests have also been conducted inside the atomic force microscope (AFM) to measure the elastic modulus of the *a*-axis (the <010> direction) GaN NWs.¹⁸ Using the MEMS-

based nanoscale testing system, Espinosa et al. have operated the in situ transmission electron microscopy (TEM) tensile experiments to characterize and compare the elastic properties of GaN NWs along different growth orientations.^{19,20} Huang et al. have used the scanning probe to punch the *a*-axis GaN NWs and observed the local plastic deformation.²¹ However, among the results of these experiments, some disagreements still remained, especially for the Young's modulus of GaN NWs.^{16–19}

In addition, planar defects such as twin boundaries (TBs) and stacking faults (SFs) are common to be found in GaN NWs. These defects are likely to enhance the physical properties of GaN NWs and make them to be building blocks of new functional devices.^{22,23} But how about the planar defects' influence on the mechanical properties of GaN NWs? Unfortunately, little efforts has been done to study this effect. Only the molecular dynamics (MD) simulations have showed that grain boundaries (GBs) could significantly lower the Young's modulus of GaN NWs.²⁴ The experimental evidence on this topic is still in absence.

Received: May 28, 2014

Revised: November 21, 2014

Published: November 26, 2014

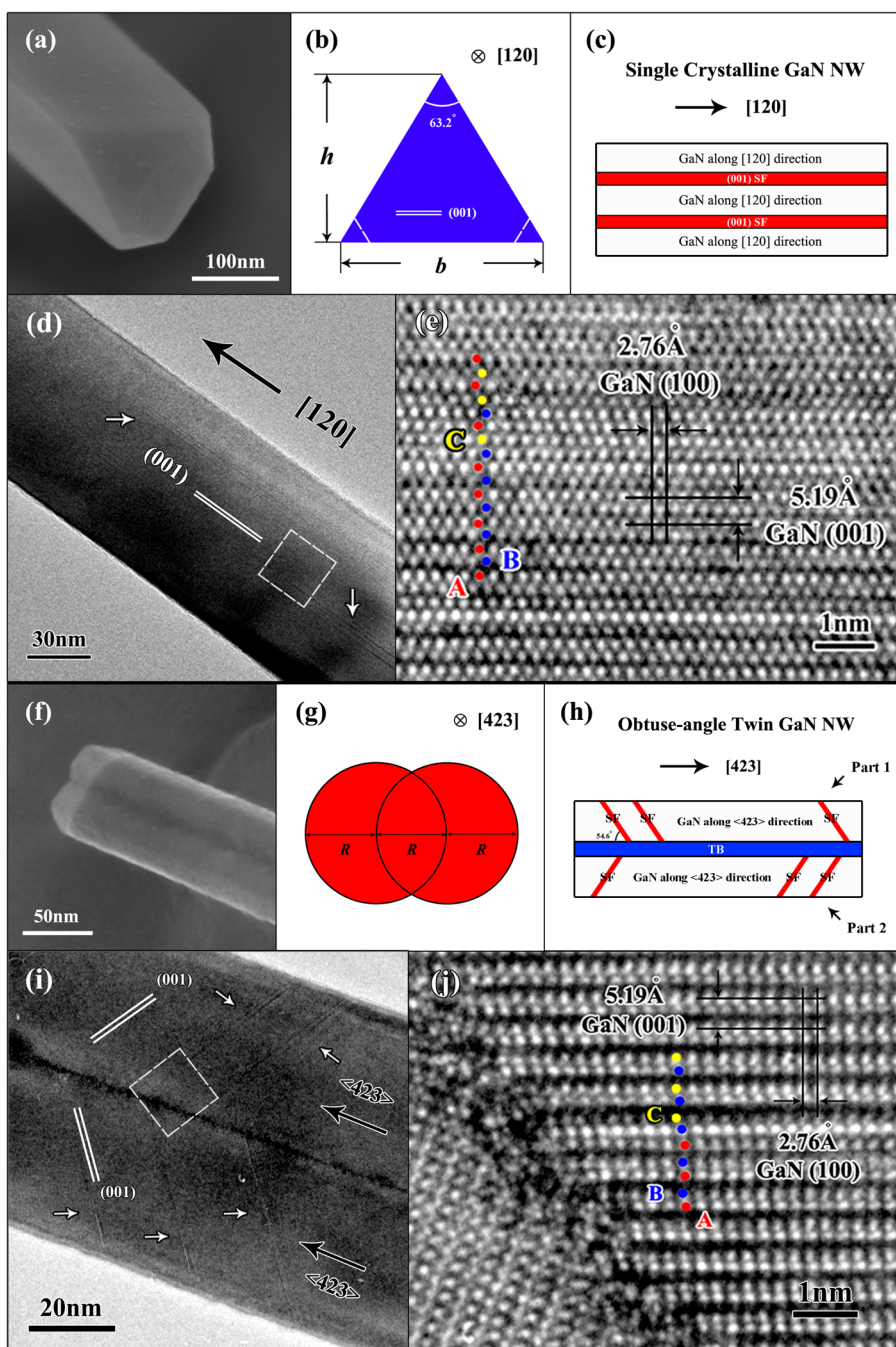


Figure 1. Typical characterization results of SC and OT GaN NWs. (a,b) The observed isosceles triangle cross section and the corresponding model of SC GaN NWs. (c) The structural model of the SC GaN NW. (d) The TEM image of an individual SC GaN NW. White arrows indicate the (001) SFs in the NW. (e) The HRTEM image collected from the white area in (d), showing the change of stacking sequence in the SC NW. (f,g) The observed dumbbell-shape cross section and the corresponding model of OT NWs. (h) The structural model of the OT NW. (i) The TEM image of an OT GaN NW. White arrows indicate the (001) SFs in the NW. (j) The HRTEM image collected from the white area in (i), showing the change of stacking sequence in OT NW.

In this paper, we investigated the elastic behavior of GaN NWs with different structures by in situ electron microscopy, especially using two different loading methods to measure the Young's modulus of twinned GaN NWs for the first time. The planar defects' effect on the elastic modulus has been revealed directly and one quantitative model based on the rules of mixtures has been established to interpret the experimental results.

Our GaN NWs were synthesized via the chemical vapor deposition (CVD) method.²⁵ Among the as-synthesized

products, high-resolution transmission electron microscopy (HRTEM) was used to find two distinct structures of GaN NWs, single crystalline (SC) NWs and obtuse-angle twin (OT) NWs.²⁵

For SC GaN NWs, the HRTEM image along [010] zone axis (Figure 1e) clearly demonstrates the single crystallinity. The measured *d*-spacing of 5.19 Å between the adjacent lattice fringes corresponds to the (001) planes, perpendicular to the [120] wire-axis in wurtzite structure. The triangular cross-section shape of this structure is presented in Figure 1a. In fact,

it is an isosceles triangle with a 63.2° apex while the base is parallel to (001) planes.^{16,17,25} The developed facets at two base angles can also be observed and were attributed to fluctuations in reaction conditions that affected the stability of the growth of a certain plane.^{16,25} As illustrated in the model of this cross section shape (Figure 1b), h and b are the height and base of the isosceles triangle, respectively.

For OT GaN NWs, the dumbbell-shape cross sections and the new twin structure with $\{304\}$ TB have already been revealed in our previous results.²⁵ The typical characterization results are presented in Figure 1f–j. The HRTEM image (Figure 1j) along $[010]$ zone axis reflects the symmetrical relationship in this bicrystalline structure. Either part on both sides of the TB grows along the $\langle 423 \rangle$ direction and the atomic profile of the $\{304\}$ TB can be referred to our former work.²⁵ Here, the dumbbell-shape cross section could be treated mathematically as the model in Figure 1g. It could be described as two circles passing through the center of each other with the radius R (see Supporting Information 1 for more details).

Meanwhile, HRTEM images also confirm the presence of (001) SFs in these two GaN structures. This kind of planar defects occurred frequently in GaN NWs and films because of the low defect energy.²⁶ In SC GaN NWs, the SFs extend parallel to the wire axis through the entire nanowire. The corresponding HRTEM image (Figure 1e) illustrates a change in stacking sequence from ABAB to ACAC. While in OT GaN NWs, the (001) SFs exist in each part of bicrystalline structure. The angle between (001) SFs and the $(30\bar{4})$ TB is 54.6° . The HRTEM image (Figure 1j) also demonstrates the profile of (001) SFs near the TB in the OT NW. On the basis of these characterization results, the models showing GaN NWs with planar defects have been established in Figure 1c,h. Red areas indicate (001) SFs and blue ones are for the TB. Moreover, the statistics of the stacking fault density have been conducted on these two structures. The results show the stacking faults density remains stable in the NWs with diameters ranging from 80 to 200 nm. The average volume percentage of (001) SFs in SC structures (V_{SF_SC}) is about 2% while the percentage in OT structures (V_{SF_OT}) is about 4%.

The well-known electric-field-induced resonance method^{17,18,27–29} was mainly employed in our experiments for measuring the Young's modulus of GaN NWs. The Young's modulus of an individual NW can be obtained according to the Euler–Bernoulli analysis of a cantilevered beam^{30–32}

$$E = \frac{\rho A}{B_1^4 I} L^4 (2\pi f_1)^2 \quad (1)$$

where constant B_1 is 1.875 for the first harmonic mode; L , A , and ρ are the length, cross-section area, and the mass density of the beam. I and f_1 are the corresponding moment of inertia and the natural resonance frequency of the beam. It is notable that the accurate measurements of beam size and the natural frequency are essential for reaching the exact Young's modulus.

The main advantage of in situ scanning electron microscopy (SEM) experiments is the convenience for manipulation, owing to the larger space in the SEM chamber. However, the resolution of SEM is limited and would not allow the precise determination of the NWs' radii and lengths, leading to errors in the final Young's modulus.¹⁹ But how about the in situ resonance experiments inside the TEM?^{16,17} It is able to acquire the accurate measurements and the structure information, but the high energy electron beam irradiation is inevitable.^{34–36} The electrostatic force resulted from the high

energy electron beam^{36,37} may also induce errors for the natural frequency f_1 . For these reasons, our developed method was designed to excite the resonant vibration in SEM and achieve the precise geometry measurements as well as the structure characterization in TEM, making the best use of these two in situ platforms.

As shown in Figure 2a, a half of the copper grid was selected as the substrate and GaN NWs were attached to the grid as

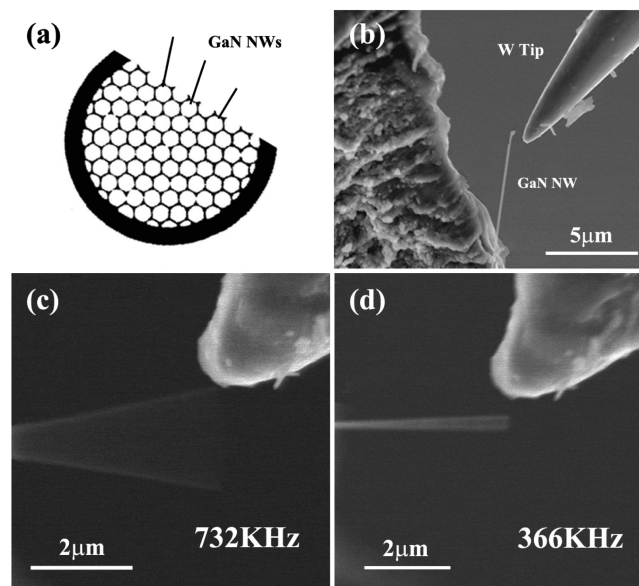


Figure 2. Developed resonance method and the excited forced resonance. (a) A schematic diagram showing a half of the copper grid as the substrate of NW cantilevers. (b) The SEM image showing the GaN NW attached on the substrate. (c) The forced resonance took place under the frequency 732 kHz. (d) The forced resonance occurred in the same nanowire in (c) under half of the frequency 366 kHz.

cantilevers by the silver paint, where the sufficient clamping area and the fixed boundary condition were ensured.³⁸ Our homemade manipulator³⁹ was mounted in the SEM (JEOL-6301F) and the sharp tungsten tip, as the counter electrode was able to achieve the three-dimensional movements and apply the alternating current (ac) and direct current (dc) signals through a signal generator. Taking the results in Figure 2c,d, for example, the off-axis force was applied by the W tip and the forced resonance was excited under the driving frequency $\Omega_1 = 732$ kHz and $\Omega_2 = 366$ kHz, respectively. According to our previous reports,³³ the forced resonance can only occur at the natural frequency f_1 and half of the natural frequency $f_1/2$. Therefore, 732 kHz could be determined as the correct natural frequency of this cantilever. Each GaN NW we chose should have an oscillatory plane almost parallel to the grid substrate. Then the maximum amplitude could be observed symmetrically in the projection plane just like the scenario in Figure 2c,d.

It is notable that the cross-section shapes of our samples, either triangular or dumbbell-like shape, has a low symmetry. Therefore, dual fundamental resonant modes in two orthogonal planes exist in either SC or OT GaN NWs, as shown in Figure 3. This phenomenon increases the difficulties and the moment of inertia (I) in eq 1 have four specific forms of expressions (Supporting Information 1) accordingly. The accurate Young's modulus could be obtained only if the SEM-observed vibrating mode was distinguished.

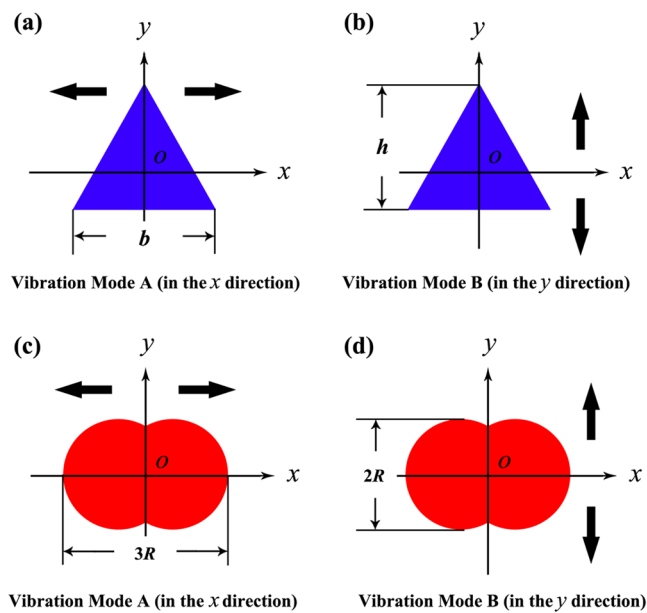


Figure 3. Vibration modes of GaN NWs with different cross-section shapes. (a,b) Vibration mode A and B of the triangle cross section shape. (c,d) Vibration mode A and B of the dumbbell-like cross-section shape.

To clarify, the half cooper grid, which fits the TEM ϕ 3 size, was transferred into the TEM (JEOL 2010) for the structure characterizations and accurate measurements after the in situ SEM resonance. The structure information on GaN NWs can be revealed directly through the selected area electron diffraction (SAED) pattern, which is an effective method to separate SC and OT structure. In the meantime, the diffraction pattern could also tell us the crystallographic orientations of the NW cantilever to the substrate. For instance, Figure 4b is the diffraction pattern of the NW cantilever in Figure 4a. The corresponding HRTEM image is also presented in Figure 4d. TEM characterization results clearly show the OT structure of this cantilever and the cross-section could be determined as the dumbbell shape. In addition, the SAED pattern also shows the

zone axis is along [010] direction. It means the [010] direction of this cantilever was perpendicular to the substrate plane. Then the previous SEM-observed oscillatory motion, which paralleled to the substrate plane, was determined as the vibration mode A of OT structure (Figure 3c). The measured NW width of 98 nm in the projecting plane corresponds to triple radius $3R$ of the dumbbell cross section. In this way, the size of the cross section was able to be measured accurately with the aid of TEM's high resolution. Here, we provide the example of the OT structure along [010] zone axis. The other three cases in Figure 3 could also be distinguished following the similar procedure.

According to the above experimental approaches, 14 GaN NWs were measured for their sizes (d , L), natural frequencies (f_1), and structure information. The diameter d is defined as the longest side of the cross-section shape. It corresponds to b in the case of SC NW or $3R$ in the case of OT NW. Aspect ratios in this work is large enough so that the transverse shear deformation is negligible for anisotropic materials¹⁶ and the Young's modulus E calculated from eq 1 is along the growth direction of the NW cantilever. All the data is listed in Table 1. Four NWs are SC structure with the growth direction [120]. The measured Young's modulus E varies from 271 to 388 GPa with an average value of 338 ± 16 GPa in the diameter range 92–110 nm. It is consistent with the reported theoretical and experimental values of bulk GaN in the same direction.^{16,17,40,41}

Notably, for the OT structures 10 GaN NWs with a wider diameter range (98–171 nm) were tested. The Young's modulus was measured from 40 to 114 GPa. The average value is only 66 ± 5 GPa. The modulus of total 14 NWs is plotted with the characteristic size d in Figure 5. It is clear that the modulus E of OT NWs shows a dramatic decrease compared to the SC ones. Espinosa et al. have used the MD simulations to reveal that the elasticity size dependence is limited to GaN NWs with diameters smaller than 20 nm.¹⁹ Therefore, the surface relaxation^{19,29} would not be dominant in our tested diameter range, which is much thicker than the critical diameter of 20 nm.

To confirm the decreasing modulus of the OT NWs the quantitative tensile tests were conducted utilizing the in situ

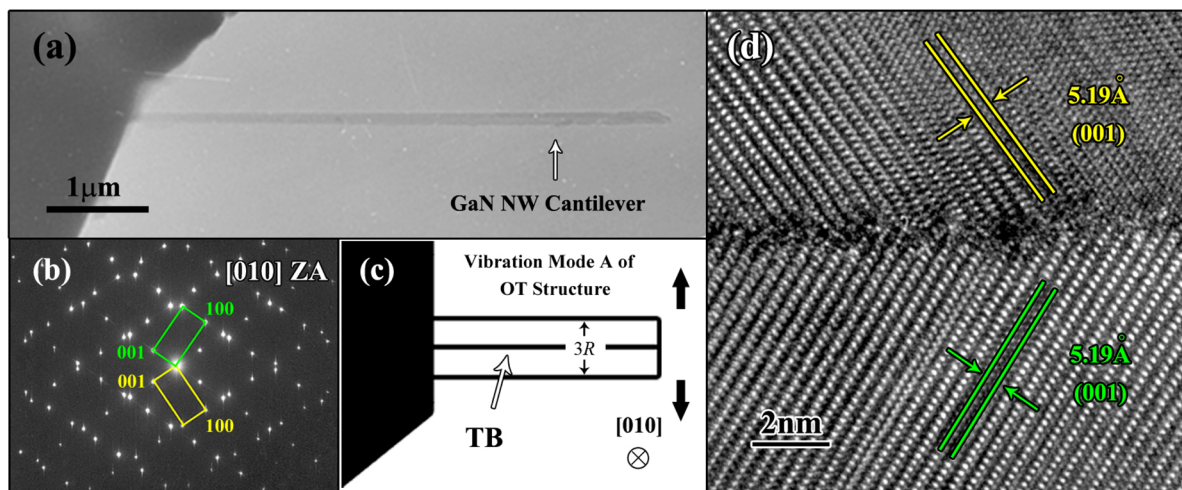


Figure 4. TEM characterization process of the GaN NW cantilever. (a) The TEM image of the NW cantilever on the substrate. (b) The SAED pattern (along [010] zone axis) of the cantilever demonstrating the OT structure. (c) The schematic diagram illustrating the crystallographic orientations of the cantilever and determines the corresponding vibration mode. (d) The HRTEM image of this GaN NW showing the OT structure.

Table 1. Measured Sizes, Resonance Frequency, Vibration Mode, and Young's Modulus of GaN Nanowires of SC and OT Structures^a

no.	natural frequency f_1 / kHz	vibration mode	length $l/\mu\text{m}$ ($\pm 0.05 \mu\text{m}$)	diameter d/nm ($\pm 2 \text{nm}$)	Young's modulus E/GPa
1	1751	A(SC)	6.68	103	271 ± 13
2	1092	A (SC)	9.56	110	388 ± 16
3	1357	B (SC)	7.34	92	336 ± 17
4	1797	B (SC)	6.68	99	355 ± 18
5	722	A (OT)	8.70	142	44 ± 3
6	365	B (OT)	10.06	150	40 ± 4
7	978	A (OT)	8.24	164	48 ± 3
8	1002	A (OT)	6.94	98	71 ± 8
9	360	B (OT)	9.94	141	42 ± 4
10	398	B (OT)	10.98	163.5	44 ± 3
11	914	B (OT)	8.87	172.5	114 ± 7
12	732	A (OT)	9.01	105	95 ± 8
13	515	A (OT)	10.70	120	72 ± 6
14	578	B (OT)	10.50	171	91 ± 6

^aThe vibration modes A and B of SC/OT structure refer to the 4 modes in Figure 3.

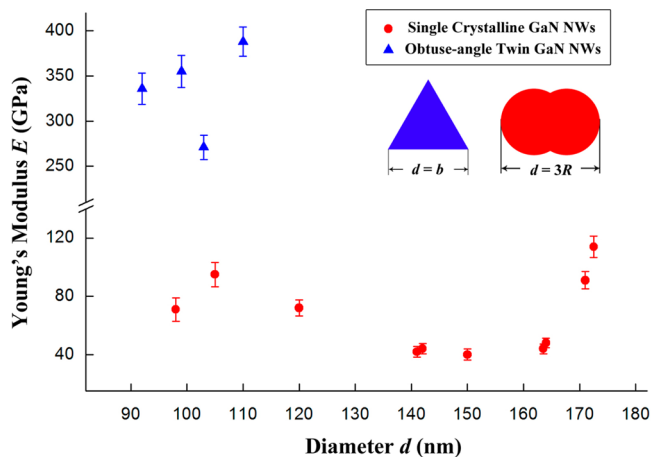


Figure 5. Young's Modulus E with Diameter d of GaN NWs from resonance experiments.

TEM nanoindentation system (PI 95 Picoindenter from Hysitron) coupled with a push-to-pull (PTP) device.^{42,43} An OT GaN NW was selected and transferred to the PTP chip using the Kleindiek Mechanical Manipulator in dual-beam FIB/SEM system (FEI Helios NanoLab). The NW with the diameter $d = 3R = 294 \text{ nm}$ was bridging the gap of the chip and two platinum (Pt) patches were deposited at both ends of the NW. During this process, only very small parts of the NW were exposed to the ion beam in order to minimize the ion irradiation damage from FIB.

While applying the tensile load inside TEM (JEOL 2100), the projected width of the NW is $2R = 196 \text{ nm}$ according to the crystallographic orientation from SAED pattern. Figure 6a is the image prior to loading and the length between two markers was defined as the original length L_0 . Figure 6b is the final state of the NW just before fracture. The longest length between the two markers here was defined as L_{max} . The elongation $\delta L = L_{\text{max}} - L_0$ was measured to be 4.8 nm and the strain ϵ was 2.5% . Movie 1 (Supporting Information 3) presents the whole process of the tensile experiment. The instant load and displacement of the indenter could be lively registered. After

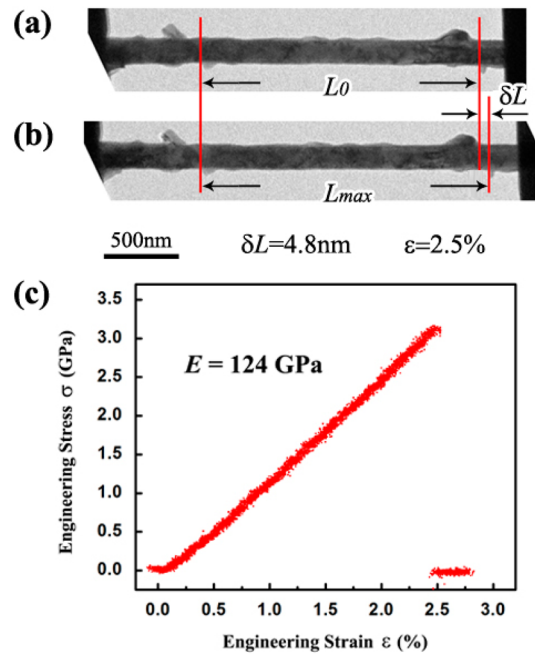


Figure 6. Tensile result of the OT GaN NW. (a) The TEM image of the NW prior to loading showing the original length L_0 . (b) The TEM image of the NW just before fracture showing the longest length L_{max} . (c) The σ - ϵ curve of the OT NW. The measured Young's modulus is 124 GPa .

subtracting the mechanical response of the PTP chip, the stress-strain behavior of this OT GaN NW is presented in Figure 6c. The σ - ϵ curve shows a linear elastic behavior and no plastic deformation was observed. In Supporting Information Movie 1, the broken end of the NW seems flat with no noticeable diameter reduction or necking. Our ultimate concern was the Young's modulus, which was measured to be $124 \pm 5 \text{ GPa}$, confirming a fall in the modulus.

Young's modulus is directly related to interatomic bonding of solids. The misorientated bonds, weak bonds, and dangling bonds induced by planar defects could lower the Young's modulus to some extent.^{44,45} Shaefer et al. have compressed the Au clusters with or without annealing and found the annealing process, eliminating TBs in the clusters could quadruple the elastic modulus.⁴⁶ Liu et al. have found the Young's modulus in WO_3 NWs lower than the bulk case and attributed it to the planar defects.⁴⁷ Nam also considered the SFs as possible origins to decrease the modulus of GaN NWs in their results.¹⁶ These reports have shown that planar defects could lower the elastic modulus in nanomaterials; however, the quantitative relationship involved in this topic has not been obtained.

Several composite models based on the rules of mixtures have already been established to describe the grain boundaries' effect on the modulus of nanocrystalline materials.^{48,49} Because of the random grain orientations, Voigt model and Reuss model⁵⁰ are always used in predicting the upper bound and the lower bound of the nanocrystalline materials' modulus.^{48,49} Our GaN NWs have the uniform orientated planar defects so that it is reasonable to use the Voigt model or Reuss model to predict their Young's modulus directly. The planar defects (SFs and TBs) can be regarded as a fiber phase embedded in the GaN crystal matrix phase. The effective modulus of the planar defects (E_{pd}) is a key issue for the prediction. However, to our present knowledge, no quantitative elastic modulus has been

measured at the planar defects experimentally. Only the theoretical simulations and calculations have revealed that E_{pd} is considerably smaller than the corresponding bulk value (E_B) and the ratio E_{pd}/E_B is only about 0.8~2.4%.^{43,51,52} Considering the bulk modulus of wurtzite-type GaN is about 280 GPa,⁴¹ the estimate for E_{pd} is about 2.3–6.7 GPa. In our opinion, the average 4.5 GPa of this range is reasonable to be used here for the discussion.

Figure 7a is the Voigt model in the rules of mixtures, describing the parallel fiber (F) and matrix (M) are stretched

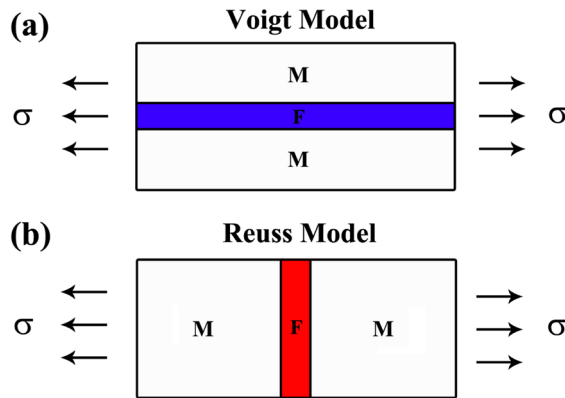


Figure 7. Schematic diagrams showing the rules of mixtures. (a) The Voigt model with the fiber parallel to the loading direction. (b) The Reuss model with the fiber perpendicular to the loading direction.

by the same amount in the loading direction. The modulus of the whole composite NW along the loading direction (E_{Voigt}) is⁵⁰

$$E_{Voigt} = E_M V_M + E_F V_F \quad (2)$$

where E_M is the modulus of the matrix phase and E_F is the modulus of the fiber along the loading direction. V_M and V_F are the volume fraction of the matrix and the fiber, respectively.

Returning to Figure 1c, (001) SFs in SC NWs are parallel to the wire axis [120]. In this scenario, the GaN crystal along [120] direction (the white area in Figure 1c) can be regarded as the matrix and the SFs can be considered as the fiber phase. Then, the Young's modulus along wire axis (E_{SC}) should be calculated as

$$E_{SC} = E_{[120]GaN} V_{[120]GaN} + E_{SF} V_{SF_SC} \quad (3)$$

where $E_{[120]GaN}$ is the modulus of GaN crystal along [120] direction. Its value can be calculated as 283 GPa based on the elastic constants of wurtzite-type GaN (see Supporting Information 4). Because the average volume percentage of (001) SFs in the tested SC structures (V_{SF_SC}) is very small, only about 2% based on our characterization results, the contribution of the item $E_{SF} V_{SF_SC}$ is very limited in eq 3. Therefore, the modulus of the SC NW could be estimated as close as the matrix value $E_{SC} \approx E_{[120]GaN} = 283$ GPa, and this is in agreement with our experimental result (338 GPa) for the SC GaN NWs.

Besides, the Reuss model in Figure 7b describes another circumstance. While the loading direction is perpendicular to the fibers, the elastic modulus of the composite model (E_{Reuss}) is⁵⁰

$$\frac{1}{E_{Reuss}} = \frac{V_F}{E_F} + \frac{V_M}{E_M} \quad (4)$$

With regard to the OT NW model in Figure 1g, Part 1 or Part 2 is the area on either side of the TB. In either part, the GaN crystal along [423] direction (the white area in Figure 1h) can be considered as the matrix while (001) SFs can be deemed as the perpendicular fiber phase equivalently. Then the modulus of Part 1 along the wire axis (E_1) should be calculated as

$$\frac{1}{E_1} = \frac{V_{SF_1}}{E_{SF}} + \frac{V_{[423]GaN_1}}{E_{[423]GaN}} \quad (5)$$

where $E_{[423]GaN}$ is the modulus of GaN crystal along [423] direction, E_{SF} is the effective modulus of (001) SF along the wire axis, and V_{SF_1} and $V_{[423]GaN_1}$ are the volume fraction of the SFs phase and matrix phase in Part 1, respectively.

For the whole OT NW model (Figure 1h) consisting of the TB, Part 1, and Part 2, the TB along the wire axis should be considered as the parallel fiber, following the Voigt model. Then the NW's modulus E_{OT} obeys the parallel combination rules of mixtures

$$E_{OT} = E_1 V_1 + E_2 V_2 + E_{TB} V_{TB} \quad (6)$$

where E_1 (or E_2) is the modulus of Part 1 (or Part 2) according to eq 5, V_1 (or V_2) is the volume percentage of Part 1 (or Part 2) to the whole OT NW, E_{TB} is the TB modulus along the wire axis and V_{TB} is the volume percentage of the TB to the whole NW.

Because V_{TB} is very limited with the value only around 1%, the contribution of the item $E_{TB} V_{TB}$ is negligible in eq 6. In addition, in view of the mirror symmetry of the twin structure the modulus E_1 and E_2 can be regarded as the same value, as well as the volume percentage V_1 and V_2 . Therefore, either the value of V_1 or V_2 is very close to 0.5. Then the elastic modulus of OT NW in eq 6 could be simplified to

$$E_{OT} = 2E_1 V_1 \approx E_1 = \frac{E_{SF} E_{[423]GaN}}{V_{SF_1} E_{[423]GaN} + V_{[423]GaN_1} E_{SF}} \quad (7)$$

In Part 1, the SFs volume fraction V_{SF_1} (as same as the SFs volume fraction V_{SF_OT} of the whole NW because of the twin symmetry) is 4% according to our characterization results and $V_{[423]GaN_1}$ is 96%. $E_{[423]GaN}$ is calculated as 272 GPa (see Supporting Information 4) and the modulus of SFs (E_{SF}) could be regarded as 4.5 GPa (the average of E_{pd}). Then the modulus of the OT nanowire could be calculated as $E_{OT} = 76$ GPa according to eq 7. This result is in great accordance with our experimental results of the OT NWs (66 ± 5 GPa).

In fact, the planar defects' influence on the modulus is always an important issue in the mechanical properties of nanomaterials. In our point of view, the classical mechanics still works for our tested GaN NWs. Both relative orientations and volume fractions of planar defects affect the NWs' elastic modulus. Which rule of mixtures (Voigt model or Reuss model) should be used is determined by the relative orientations of planar defects in NWs. Also, what extent the effect is depends on the volume percentage of the planar defects. This point of view can also be supported by some other reports. For instance, Tao et al. have performed the nanoindentation tests on the $Mg_2B_2O_5$ NWs with (010) TBs.⁵³ The axial elastic modulus just showed a slight decrease in the NWs where the limited TBs are parallel to the wire axis. On the basis of our analysis, the role of parallel TBs is as similar as the parallel fiber in Voigt model and the softening effect on the modulus is not obvious according to eq 2. Moreover, Wang et al. have investigated the elastic properties of biaxial SiC-SiO_x NWs and found the modulus of the biaxial

structures was only around 60 GPa with no size dependence;⁵⁴ people may have the question why the modulus result (60 GPa) was either lower than that of single crystalline SiC NW (>300 GPa) or SiO_x NW (60–100 GPa) at the same diameter. From their characterizations of the SiC part, it is clear that SFs that are at the angle of 64° with the wire axis existed in large quantity. Therefore, the influence of these planar defects would cause a sharp drop of the wire modulus according to the Reuss model. Hence, we think the rules of mixtures, describing the influence of planar defects on elastic modulus, may be general and valuable for other one-dimensional nanomaterials.

To summarize, the elastic properties of GaN nanowires with different structures (SC and OT structures) have been investigated utilizing the developed in situ resonance method. Meanwhile, the modulus of new OT GaN NWs has been confirmed via in situ tensile test. In SC GaN NWs ($d > 92$ nm), the average Young's modulus is 338 ± 16 GPa, close to the bulk value. (001) SFs parallel to the wire axis could be regarded as the parallel fibers in the Voigt rule of mixtures and the limited quantity of SFs do not have an obvious influence on the wire modulus. While for OT GaN NWs, the Young's modulus is only about 66 ± 5 GPa with the diameter ranging from 98 to 171 nm. The angle between (001) SF and OT wire axis is 54.6° so that the influence on the modulus follows the Reuss model and the wire modulus decreases dramatically. In our opinion, the rules of mixtures still remain effective in our tested GaN NWs and may be extended to some other one-dimensional nanomaterials. The quantitative analysis and the experimental evidence in this work may help people better understand the relationship between defects and elastic properties at nanoscale. The SFs' effect on the elastic properties also indicates that one may construct new type of functional devices through planar defects engineering.

■ ASSOCIATED CONTENT

📄 Supporting Information

Mathematical calculations of the GaN NWs' cross-sectional areas and the moment of inertia, validation of the Euler-Bernoulli assumptions for the GaN nanowires, supplementary movie, calculations of Young's modulus of bulk wurtzite GaN along given directions, additional figures, and references. This material is available free of charge via the Internet at <http://pubs.acs.org>.

■ AUTHOR INFORMATION

Corresponding Author

*E-mail: jzhu@mail.tsinghua.edu.cn. Fax: +8610-62772507. Tel: +8610-62794026.

Notes

The authors declare no competing financial interest.

■ ACKNOWLEDGMENTS

This work was financially supported by National 973 Project of China (2009CB623701) and Chinese National Nature Science Foundation (11374174, 51390471). This work made use of the resources of the Beijing National Center for Electron Microscopy and CAMP-Nano. The authors thank Dr. Zhiping Xu from Tsinghua University for his helpful discussion.

■ REFERENCES

- (1) Nakamura, S.; Pearton, S.; Fasol, G. *The Blue Laser Diode: The Complete Story*; Springer-Verlag: Berlin, 2000.
- (2) Shul, R. J.; Vawter, G. A.; Willison, C. G.; Bridges, M. M.; Lee, J. W.; Pearton, S. J.; Abernathy, C. R. *Solid-State Electron.* **1998**, *42*, 2259.
- (3) Morkoç, H. *Handbook of Nitride Semiconductors and Devices*; Wiley-VCH: Weinheim, 2008.
- (4) Beach, R. A.; McGill, T. C. *J. Vac. Sci. Technol., B* **1999**, *17*, 1753.
- (5) Nakamura, S. *Science* **1998**, *281*, 956.
- (6) Pearton, S.; Ren, F. *Adv. Mater.* **2000**, *12*, 1571.
- (7) Uenoyama, T. *Phys. Rev. B* **1995**, *51*, 10228.
- (8) Huang, Y.; Duan, X.; Cui, Y.; Lauhon, L. J.; Kim, K. H.; Lieber, C. M. *Science* **2001**, *294*, 1313.
- (9) Johnson, J. C.; Choi, H. J.; Knusten, K. P.; Schaller, R. D.; Yang, P.; Saykally, R. J. *Nat. Mater.* **2002**, *1*, 106.
- (10) Huang, Y.; Duan, X. F.; Cui, Y.; Lieber, C. M. *Nano Lett.* **2002**, *2*, 101.
- (11) Xia, Y.; Yang, P.; Sun, Y.; Wu, Y.; Mayers, B.; Gates, B.; Yin, Y.; Kim, F.; Yan, H. *Adv. Mater.* **2003**, *15*, 353.
- (12) Zhong, Z.; Qian, F.; Wang, D.; Lieber, C. M. *Nano Lett.* **2003**, *3*, 343.
- (13) Qian, F.; Li, Y.; Gradecak, S.; Wang, D. L.; Barrelet, C. J.; Lieber, C. M. *Nano Lett.* **2004**, *4*, 1975.
- (14) Huang, C. T.; Song, J.; Lee, W. F.; Ding, Y.; Gao, Z.; Hao, Y.; Chen, L. J.; Wang, Z. L. *J. Am. Chem. Soc.* **2010**, *132*, 4766.
- (15) Gao, Y.; Wang, Z. L. *Nano Lett.* **2009**, *9*, 1103.
- (16) Nam, C. Y.; Jaroenapibal, P.; Tham, D.; Luzzi, D. E.; Evoy, S.; Fischer, J. E. *Nano Lett.* **2006**, *6*, 153.
- (17) Henry, T.; Kim, K.; Ren, Z.; Yerino, C.; Han, J.; Tang, H. X. *Nano Lett.* **2007**, *7*, 3315.
- (18) Ni, H.; Li, X. D. *J. Mater. Res.* **2006**, *21*, 2882.
- (19) Bernal, R. A.; Agrawal, R.; Peng, B.; Bertness, K. A.; Sanford, N. A.; Davydov, A. V.; Espinosa, H. D. *Nano Lett.* **2011**, *11*, 548.
- (20) Minary-Jolandan, M.; Bernal, R. A.; Kuljanishvili, I.; Parpoli, V.; Espinosa, H. D. *Nano Lett.* **2012**, *12*, 970.
- (21) Huang, J. Y.; Zheng, H.; Mao, S. X.; Li, Q.; Wang, G. T. *Nano Lett.* **2011**, *11*, 1618.
- (22) Liu, B.; Bando, Y.; Tang, C.; Xu, F.; Hu, J.; Golberg, D. *J. Phys. Chem. B* **2005**, *109*, 17082.
- (23) Chen, Z.; Cao, C.; Zhu, H. *Chem. Vap. Deposition* **2007**, *13*, 527.
- (24) Xie, S. F.; Chen, S. D.; Soh, A. K. *Chin. Phys. Lett.* **2011**, *28*, 066201.
- (25) Dai, S.; Zhao, J.; He, M.; Wu, H.; Xie, L.; Zhu, J. *J. Phys. Chem. C* **2013**, *117*, 12895.
- (26) Tham, D.; Nam, C. Y.; Fischer, J. E. *Adv. Funct. Mater.* **2006**, *16*, 1197.
- (27) Poncharal, P.; Wang, Z. L.; Ugarte, D.; de Heer, A. W. *Science* **1999**, *283*, 1513.
- (28) Suryanvashi, A. P.; Yu, M. F.; Wen, J.; Tang, C.; Bando, Y. *Appl. Phys. Lett.* **2004**, *84*, 2527.
- (29) Chen, C. Q.; Shi, Y.; Zhang, Y. S.; Zhu, J.; Yan, Y. J. *Phys. Rev. Lett.* **2006**, *96*, 075505.
- (30) Meirovich, L. *Element of Vibration Analysis*; McGraw-Hill: New York, 1986.
- (31) Gere, J. M.; Timoshenko, S. P. *Mechanics of Materials*; PWS Pub. Co: Boston, 1997.
- (32) Timoshenko, S. P.; Gere, J. M. *Theory of Elastic Stability*; McGraw-Hill: New York, 1961.
- (33) Shi, Y.; Chen, C. Q.; Zhang, Y. S.; Zhu, J.; Yan, Y. J. *Nanotechnology* **2007**, *18*, 075709.
- (34) Moore, N. W.; Luo, J.; Huang, J. Y.; Mao, S. X.; Houston, J. E. *Nano Lett.* **2009**, *9*, 2295.
- (35) Zheng, K.; Wang, C. C.; Cheng, Y. Q.; Yue, Y. H.; Han, X. D.; Zhang, Z.; Shan, Z. W.; Mao, S. X.; Ye, M. M.; Yin, Y. D.; Ma, E. *Nat. Commun.* **2010**, *1*, 24.
- (36) Dai, S.; Zhao, J.; Xie, L.; Cai, Y.; Wang, N.; Zhu, J. *Nano Lett.* **2012**, *12*, 2379.
- (37) Zhang, Y.; Wang, N.; He, R.; Zhang, Q.; Yan, Y.; Zhu, J. *J. Mater. Res.* **2000**, *5*, 1048.
- (38) Qin, Q.; Xu, F.; Cao, Y.; Ro, P. I.; Zhu, Y. *Small* **2012**, *8*, 2571.
- (39) Yan, Y. J.; Zhang, Y. S.; Peng, K. Q.; Zhu, J. *Chin. Electron Microsc. Soc.* **2004**, *23*, 484.

- (40) Kim, K.; Lambrecht, R. L.; Segall, B. *Phys. Rev. B* **1994**, *50*, 1502.
- (41) Wright, A. F. *J. Appl. Phys.* **1997**, *82*, 2833.
- (42) Oh, Y.; Cyrankowski, E.; Shan, Z. W.; Asif, S. A. S. *Micro/Nano-Mechanical Test System Employing Tensile Test Holder with Push-to-Pull Transformer*. U.S. Patent Application number 20100095780.
- (43) Guo, H.; Chen, K.; Oh, Y.; Wang, K.; Dejoie, C.; Asif, S. A. S.; Warren, O. L.; Shan, Z. W.; Wu, J.; Minor, A. M. *Nano Lett.* **2011**, *11*, 3207.
- (44) Schiøtz, J.; Di Tolla, F. D.; Jacobsen, K. W. *Nature* **1998**, *391*, 561.
- (45) Kluge, M. D.; Wolf, D.; Lutsko, J. F.; Phillpot, S. R. *J. Appl. Phys.* **1990**, *67*, 2370.
- (46) Shaefer, D. M.; Patil, A.; Andres, R. P. *Phys. Rev. B* **1995**, *51*, 5322.
- (47) Liu, K. H.; Wang, W. L.; Xu, Z.; Liao, L.; Bai, X. D.; Wang, E. G. *Appl. Phys. Lett.* **2006**, *89*, 221908.
- (48) Chaim, R. *J. Mater. Res.* **1997**, *12*, 1828.
- (49) Yeheskel, O.; Chaim, R.; Shen, Z.; Nygren, M. *J. Mater. Res.* **2005**, *20*, 719.
- (50) Bertholet, J. M. *Composite Materials: Mechanical Behavior and Structural Analysis*; Springer: New York, 1998.
- (51) Xu, T.; Zheng, L. *Philos. Mag. Lett.* **2004**, *84*, 225.
- (52) Zheng, L.; Xu, T. *Mater. Sci. Technol.* **2004**, *20*, 605.
- (53) Tao, X.; Li, X. *Nano Lett.* **2008**, *8*, 505.
- (54) Wang, Z. L.; Dai, Z. R.; Gao, R. P.; Bai, Z. G.; Gole, J. L. *Appl. Phys. Lett.* **2000**, *77*, 3349.